metals

MDPI

Article

Numerical Analysis on Temperature Field of Grinding Ti-6Al-4V Titanium Alloy by Oscillating Heat Pipe Grinding Wheel

Ning Qian [1,†], Zhengcai Zhao [1,†], Yucan Fu [1,*], Jiuhua Xu [1] and Jiajia Chen [2]

[1] College of Mechanical and Electrical Engineering, Nanjing University of Aeronautics and Astronautics, Nanjing 210016, China; n.qian@nuaa.edu.cn (N.Q.); zhengcaizhao@nuaa.edu.cn (Z.Z.); jhxu@nuaa.edu.cn (J.X.)

[2] College of Mechanical and Electronic Engineering, Nanjing Forestry University, Nanjing 210037, China; jiajiachen@njfu.edu.cn

* Correspondence: yucanfu@nuaa.edu.cn; Tel.: +86-025-8489-5857

† These two authors contribute equally to this work.

Received: 28 April 2020; Accepted: 17 May 2020; Published: 21 May 2020

Abstract: When grinding hard-to-machining materials such as titanium alloys, a massive grinding heat is generated and gathers in the grinding zone due to the low thermal conduction of the materials. The accumulated grinding heat easily leads to severe thermal damages to both the workpiece and the grinding wheel. A novel oscillating heat pipe (OHP) grinding wheel is one of the solutions to this phenomenon. The oscillating heat pipe grinding wheel can transfer the grinding heat directly from the grinding zone to avoid heat accumulation and a high temperature rise. In this paper, the temperature field of the grinding Ti-6Al-4V alloy is investigated, via the oscillating heat pipe grinding wheel, by numerical analysis. The three-dimensional thermal conduction model is built accordingly, containing the grinding wheel, grinding zone and Ti-6Al-4V workpiece. Due to the enhanced heat transport capacity of the oscillating heat pipe grinding wheel, the highest temperature in the grinding zone and the temperature on the ground surface of the workpiece decrease dramatically. For example, under a grinding heat flux of 1×10^7 W/m^2, when using the grinding wheel without OHP and with OHPs, the highest temperature in the grinding zone drops from 917 °C to 285 °C by 68.7%, and the ground surface temperature decreases from 823 °C to 244 °C by 71.2%. Moreover, the temperature distribution on the grinding wheel is more uniform with an increase of the number of oscillating heat pipes.

Keywords: oscillating heat pipes; grinding wheel; temperature field; simulation; titanium alloy

1. Introduction

Hard-to-machining materials, such as titanium alloys, superalloys and composites, etc., are widely used in turbomachinery components [1]. Due to the high strength or high hardness and low thermal conduction of the materials, grinding these materials encounters some problems [2]. A massive heat is generated during the grinding process, and the heat easily gathers in the grinding zone due to the low conduction of the grinding wheel and workpieces [3–6]. The accumulated grinding heat will lead to a local high temperature on the workpiece ground surface and cause surface and sub-surface thermal damages. On the other hand, the grinding heat will make the grinding wheel wear faster and more severely. As a result, the grinding quality and the grinding efficiency are low and the cost is high. The machining cost indexes of titanium alloys and superalloys are as high as 5.1 and 3.4, while the machining cost index of aluminum alloys is only 0.4 [7].

Given all these problems, many studies have been conducted on the grinding parameters, grinding wheel or cooling method perspectives. Some superabrasive (e.g., diamond or cubic boron nitride) grinding wheels are made by vitrifying [8–10] or electroplating [11–13] methods to increase the sharpness of the grinding wheel to reduce the grinding forces [14]. Some brazed superabrasive grinding wheels are developed to further decrease the specific grinding energy and improve the cooling condition [12]. To improve the lubrication to reduce the grinding force and heat, solid lubrications, such as graphene [15], CeO_2 [16] or h-BN [17], are added in the abrasive layer of the grinding wheel. Moreover, minimum quantity lubrication (MQL) has also been introduced lately [18–21]. Additionally, for a better cooling effect, some nanofluids are combined with MQL for the grinding processes [22–27]. To bring out the grinding heat from the grinding zone, different coolants are developed, such as water-based coolants or oil-based coolants. Besides, the coolant delivery methods are improved from the conventional high-volume low-velocity flood delivery [28,29] to high-pressure coolant delivery [30] or cryogenic cooling [20,31–33], etc. Internal coolant delivery systems [34,35] and the modification of nozzles [36,37] are also introduced to increase the cooling effect. Another method, continuous dressing, is also applied to maintain the sharpness of the grinding wheel in order to avoid grinding burn-out [38,39]. However, with the mentioned methods it is fundamentally difficult to solve the grinding heat problem, because the methods only improve the heat transfer during the grinding process to a limited extent rather than change the heat transfer mechanism. The grinding heat still relies on the coolant to be brought out. Due to the closure of the grinding zone and the air barrier close to the high-rotating grinding wheel, only a small amount of coolant will enter the grinding zone to bring out the grinding heat, and the rest of the coolant is consequently wasted [40]. Therefore, a novel method is needed to enhance the heat transfer in the grinding zone, so that the massive grinding heat will avoid accumulating in the grinding zone and causing a high temperature and thermal damages.

The oscillating heat pipe (OHP) is a novel passive thermal device that can transfer heat highly efficiently without external driving [41–43]. OHPs have a high heat transport capacity, and the thermal resistance of OHPs can be as low as 0.1 K/W [44–46]. Owing to the high thermal transfer performance, OHPs are inserted in the cutting tool to transfer the cutting heat in time to avoid burn-out [47,48]. The concept of the oscillating heat pipe grinding wheel (OHP grinding wheel) was introduced in the previous studies. The OHPs are fabricated inside the grinding wheel, so that the grinding heat can be transferred directly through the grinding wheel instead of accumulating in the grinding zone. The heat transport capacity [43,49] and the design method [50] are studied. When using the OHP grinding wheel, the whole grinding heat transfer paths can be different, which will change the overall temperature distribution. To investigate the temperature distribution on the grinding wheel and the workpiece, grinding titanium alloy by the OHP grinding wheel is modelled by three-dimensional simulation in this paper.

2. Simulation Model and Parameters

2.1. OHP Grinding Wheel Model

The design of the OHP grinding wheel mainly includes the design of oscillating heat pipe channels and the overall structure. According to the heat transport capacity investigation completed by the authors, the inner diameter of the oscillating heat pipe is recommended as 3 mm for the beat thermal performance. Additionally, the oscillating heat pipes are positioned on the plane parallel to the rotational axis of the grinding wheel. In this case, centrifugal acceleration caused by the rotation does not segregate the fluid between the evaporator and condenser, and the rotation benefits the improvement of the heat transfer [51–55]. The oscillating heat pipe channels are formed by several straight holes along the axis direction and connected grooves, as shown in Figure 1. Then, the top and bottom grooves will be welded with blind flanges to form the multi-loop oscillating heat pipes. The abrasive layer (also the evaporator of the OHP grinding wheel) is 20 mm high, and the condenser of the OHP grinding wheel is as high as the abrasive layer. The adiabatic section of the OHP grinding

wheel is 15 mm high. The evaporator, condenser and the adiabatic section are the terms in the oscillating heat pipe field, the evaporator and condenser are the place where heat is transferred in and out, while the adiabatic section is where there is no heat exchange. Moreover, eight 1.5 mm-thick and 7 mm-high fins are fabricated on the condenser for enhanced heat dissipation.

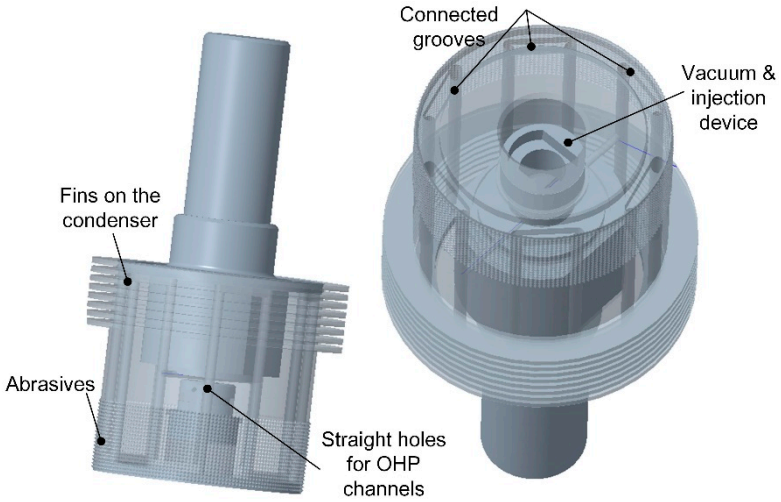

Figure 1. The design of the oscillating heat pipe (OHP) grinding wheel (the matrix is set as transparent for a better illustration).

2.2. Simulation Model

The grinding Ti-6Al-4V titanium alloy by the OHP grinding wheel is simulated as illustrated in Figure 2. The workpiece, OHP grinding wheel, as well as the grinding zone are modelled. The oscillating heat pipes are fabricated inside the grinding wheel, as shown in Figure 2.

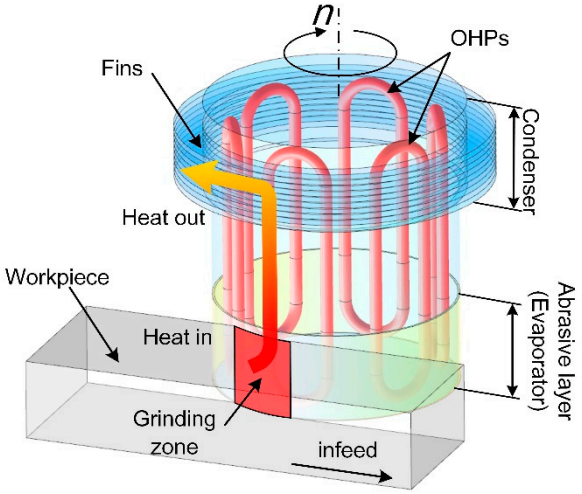

Figure 2. Simulation model illustration: grinding with the OHP grinding wheel.

In this simulation, a grinding wheel with a diameter of 60 mm and length of 82 mm is modelled. Four OHP grinding wheels are modelled, namely grinding wheels with non-OHPs, 2 OHPs, 4 OHPs and 6 OHPs. The OHP is a single-loop closed oscillating heat pipe with a diameter of 3 mm and length of 78 mm. Besides, the evaporator and condenser of the OHP are both 20 mm long. According to the thermal performance studies of single-loop closed OHPs, acetone is chosen as the working fluid for its good heat transport capacity [43,49,50,55]. In the condenser region of the OHP grinding wheel,

eight fins are used for the enhancement of heat transfer. The workpiece is 100 mm long and 20 mm high, which is the same as the height of the abrasive layer of the grinding wheel. The depth of the cut is 0.5 mm. Additionally, the grinding zone is the contact surface between the grinding wheel and the workpiece, which is also modelled, as shown in Figure 2. The grinding wheel and the workpiece in the grinding zone are in face-contact. As for the abrasive layer, the abrasive layer of the grinding wheel is a monolayer of brazed cubic boron nitride (CBN) by Ag-Cu-Ti filler. The CBN abrasives are in 40/50 mesh, with effective diameters of 0.355–0.425 mm. The abrasive layer is measured as around 0.5 mm thick. Therefore, in the simulation, the thickness of the abrasive layer is modelled as 0.5 mm.

The mesh of the simulation model is created by ANSYS ICEM (ANSYS 18.0, ANSYS China, Shanghai, China). The mesh model is a combination of structured and unstructured mesh for good accuracy and efficiency. The workpiece is created by structured hexahedral mesh, while the OHP grinding wheel is more complicated; it is created by unstructured tetrahedral mesh. Moreover, the mesh of the grinding zone is refined, as shown in Figure 3. The quality of the mesh is checked and improved to ensure that the minimum volume of mesh is over 0 and the average mesh quality index is more than 0.7.

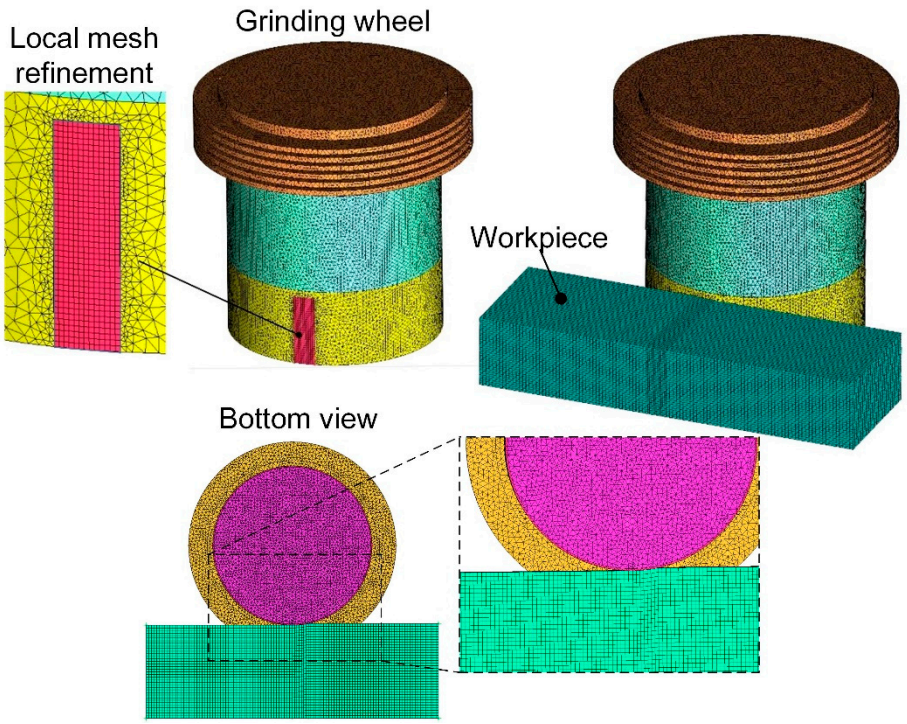

Figure 3. Mesh model.

2.3. Simulation Parameters

The grinding wheel is a brazed monolayer of CBN grains (80/100#), the workpiece is a Ti-6Al-4V block. The grinding speed varies from 15–60 m/s, the infeed speed is 120 mm/min and the depth of cut is 0.5 mm. The total grinding heat flux can be calculated as:

$$Q_{total} = \frac{F_t \cdot v_s}{l_s \cdot a_p}, \tag{1}$$

where Q_{total} is the total grinding heat flux, F_t is the tangential grinding force, b is the width of the grinding zone and l_s is the length of the grinding zone, which can be calculated as:

$$l_s = \sqrt{a_p \cdot d_s}, \tag{2}$$

where a_p is the depth of cut and d_s is the diameter of the OHP grinding wheel. Additionally, the length of the grinding zone is 5.48 mm in this case. Furthermore, the total grinding heat flux can be determined based on Equation (1) and data from reference [56]. The total grinding heat flux varies from 3.11×10^6–8.77×10^6 W/m^2. Therefore, in the simulation, the heat flux in the grinding zone is modelled by the rectangle heat source model and is set as 3×10^6 W/m^2, 5×10^6 W/m^2, 8×10^6 W/m^2 and 1×10^7 W/m^2. Furthermore, the grinding heat flux is uniformly loaded on the grinding zone.

The material of the OHP grinding wheel is 2Cr13 stainless steel. The abrasive layer is the monolayer brazed CBN grain, and the braze alloy is Ag-Cu-Ti alloy. The thermal conduction of the abrasive layer with a 1.5 mm thick 2Cr13 matrix is measured through a transient hot-line method (see Figure 4), and the conduction is 11.75 W/(m·K). Therefore, the thermal conduction of the abrasive layer can be calculated by the equivalent thermal conduction model, as shown in Figure 5. The total thickness (L_{total}), thickness of the matrix (L_m) and abrasive layer (L_a) are 3 mm, 1.5 mm and 1.5 mm, respectively. Additionally, the conduction of the 2Cr13 matrix is 18.2 W/(m·K). Hence the conduction of the abrasive layer can be calculated as 99 W/(m·K).

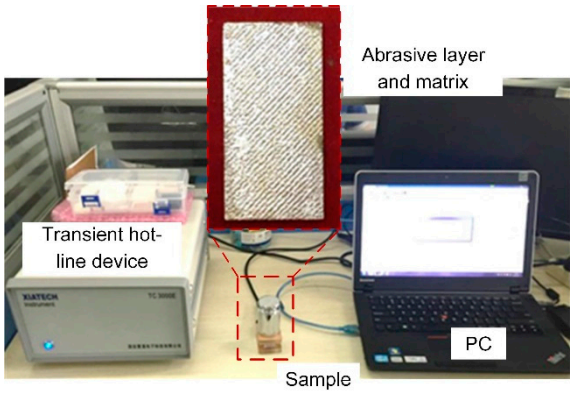

Figure 4. Thermal conduction measurement of the abrasive layer with matrix.

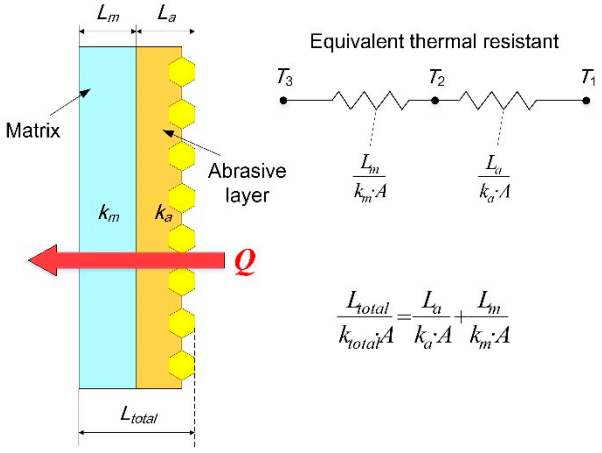

Figure 5. Thermal conduction through the abrasive layer.

The properties of the workpiece and grinding wheel materials are summed up in Table 1.

The oscillating heat pipes inside the OHP grinding wheel are filled with acetone and have a maximum effective heat transfer coefficient of 2699 W/(m^2·K) [43,50,55]. In this simulation, the equivalent thermal conduction of the OHP is determined as follows:

$$k_{OHP} = \frac{P}{N \cdot \left(\frac{\pi d_0^2}{4}\right)} \cdot \left(\frac{\Delta y}{\Delta T}\right), \quad (3)$$

where k_{OHP} is the equivalent thermal conduction of the OHP, P is the heating power, N is the number of OHP channels, d_0 is the diameter of the OHP, Δy is the distance between the evaporator and condenser of the OHP and ΔT is the temperature difference between the evaporator and condenser. In this case, the maximum k_{OHP} is 8900 W/(m·K).

Table 1. Physical properties.

Material	Density	Specific Capacity	Thermal Conduction
	kg/m^3	J/(kg·K)	W/(m·K)
2Cr13 stainless steel	8030	502.5	18.2
Ti-6Al-4V alloy	4440	674	9.8
Abrasive layer	8000	509	99

In addition, the boundary conditions and solver for this simulation are tabulated in Table 2, and the parameters are set in ANSYS FLUENT (ANSYS 18.0, ANSYS China, Shanghai, China) for solutions.

Table 2. Simulation setups.

Parameters	Value
Ambient and initial temperature (°C)	15
Environment pressure (atm)	1
Thermal convection for condenser (W/(m^2·K))	700
Solver	Segregated solver
Time step (s)	0.005

3. Results and Discussion

The simulation considers the dry-grinding Ti-6Al-4V alloy by the OHP grinding wheel. When the iteration residual is less than 10^{-5}, a stable result is achieved. The influences of the grinding heat and heat transfer ability of the OHP grinding wheel on the temperature field of the grinding wheel and workpiece are involved and discussed in this section.

3.1. Effects of the Grinding Heat Flux and OHPs

The grinding heat flux increases from 3×10^6 W/m^2 to 1×10^7 W/m^2. The highest temperature in the grinding zone is captured as shown in Figure 6. With the increase of the grinding heat flux, the highest temperature in the grinding zone rises almost linearly. Additionally, the grinding wheel without OHPs generates the highest temperature, followed by the grinding wheel with 2 and 4 OHPs, and the grinding wheel with 6 OHPs has the lowest temperature. In addition, it is clear that the OHP has an excellent thermal transfer effect for the grinding process. Under a grinding heat flux of 3×10^6 W/m^2, the highest temperature caused by the grinding wheel with 6 OHPs is 99 °C, while the temperature generated by the grinding wheel without OHP is 258 °C, 2.6 times the temperature generated by the grinding wheel with 6 OHPs. When the grinding heat flux reaches 1×10^7 W/m^2, the highest temperature caused by the grinding wheel with 6 OHPs is just 286 °C; however, the temperature caused by the grinding wheel without OHP rises as high as 917 °C, which can lead to severe thermal damages.

As for the grinding wheel with 6 OHPs, the outer surface temperature rises with the increase of the grinding heat flux. The temperature on the outer surface along the axial direction is shown in Figure 7a. Besides, the temperature difference between the average temperature of the evaporator and condenser also rises from 70 °C to 220 °C, along with the increase of the grinding heat flux, as shown in Figure 7b.

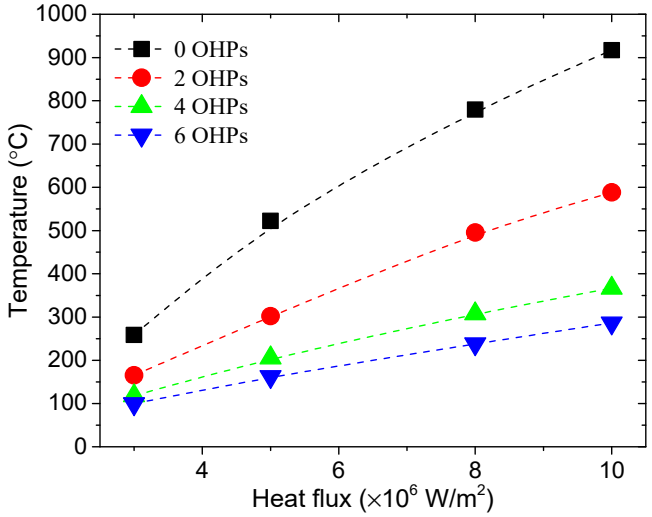

Figure 6. The highest temperature in the grinding zone under different grinding heat flux values.

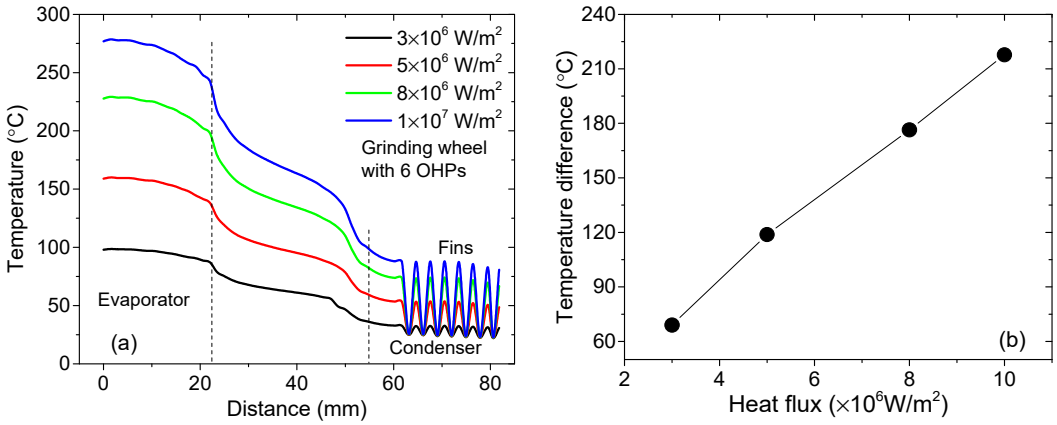

Figure 7. Temperature of the grinding wheel under different heat flux values (**a**) along the axial direction, and (**b**) the temperature difference between the evaporator and condenser.

Under the highest grinding heat flux of 1×10^7 W/m^2, the temperature fields generated by the four OHP grinding wheels are shown in Figure 8. Due to the thermal load in the grinding wheel, the abrasive layer has a higher temperature. When grinding via the grinding wheel without OHP, the grinding heat is difficult to transfer out of the grinding zone. Consequently, the heat gathers in the grinding zone and the temperature is the highest. When OHP grinding wheels are applied, owing to the high heat transport capacity of the OHP, the grinding heat is transferred out through OHPs with high efficiency. As a result, there is a significant temperature drop in the grinding zone, on the abrasive layer of the grinding wheel and workpiece. Meanwhile, the condenser of the grinding wheel has a temperature rise, which is good for the heat transfer. More OHPs can enhance the heat transfer and increase the temperature controllability of the grinding wheel. However, because of the limitations of the internal space and manufacturing costs, it is not beneficial to increase the number of OHPs blindly. In this case, the grinding wheel with at least 4 OHPs can keep the temperature under 400 °C when grinding Ti-6Al-4V alloy; for a better effect, the grinding wheel with 6 OHPs is recommended.

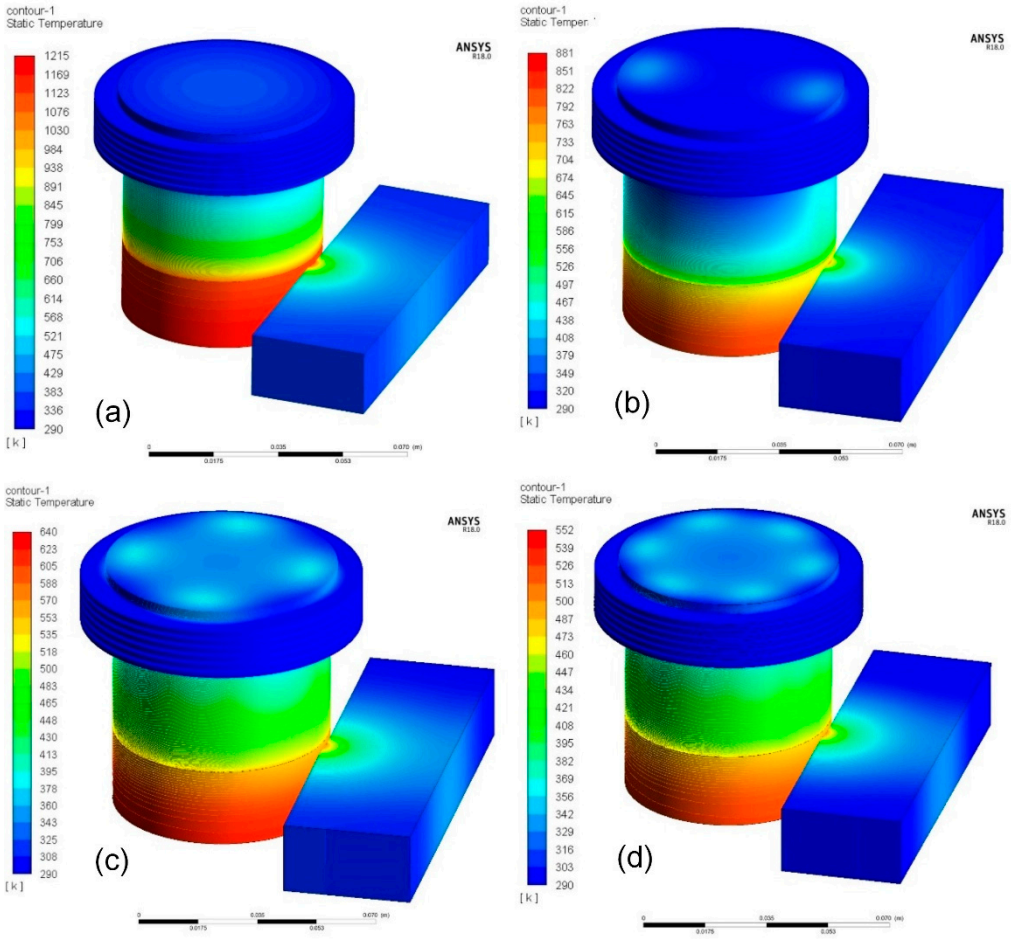

Figure 8. Temperature distribution under a grinding heat flux of 10^7 W/m^2: (**a**) non-OHP, (**b**) 2 OHPs, (**c**) 4 OHPs and (**d**) 6 OHPs (Temperature unit: K).

3.2. Temperature Field of the Grinding Wheel

To analyze the heat transport process by the OHP grinding wheel, the temperature field on the grinding wheel is focused on in this section.

When there is no OHP in the grinding wheel, the grinding heat transfers through the abrasive layer (99 W/(m·K)) and gathers in the matrix of the grinding wheel because of the low thermal conduction, 18.2 W/(m·K). Therefore, the abrasive layer of the grinding wheel has a high temperature at the range of 984 K (711 °C) to 1215 K (942 °C). Additionally, there is a significant temperature difference between the condenser and the evaporator regions of the grinding wheel, as shown in Figure 9a. When OHP grinding wheels are applied, the temperature in the grinding zone and the abrasive layer can be effectively controlled. Owing to the excellent heat transfer performance, the grinding heat can be transferred through the OHPs from the abrasive layer to the condenser and then to the environment via fins. The more OHPs are used, the lower the temperature in the abrasive layer is. Therefore, the temperature in the abrasive layer changes from the range of 733 K (460 °C) to 881 K (608 °C) to the range of 487 K (214 °C) to 552 K (279 °C) when using the grinding wheel with 2 OHPs and 6 OHPs, as shown in Figure 9. From the outer surface temperature, the temperature on the region between the evaporator and condenser gets more and more uniform when a larger number of OHPs are used, as illustrated in Figure 9b–d.

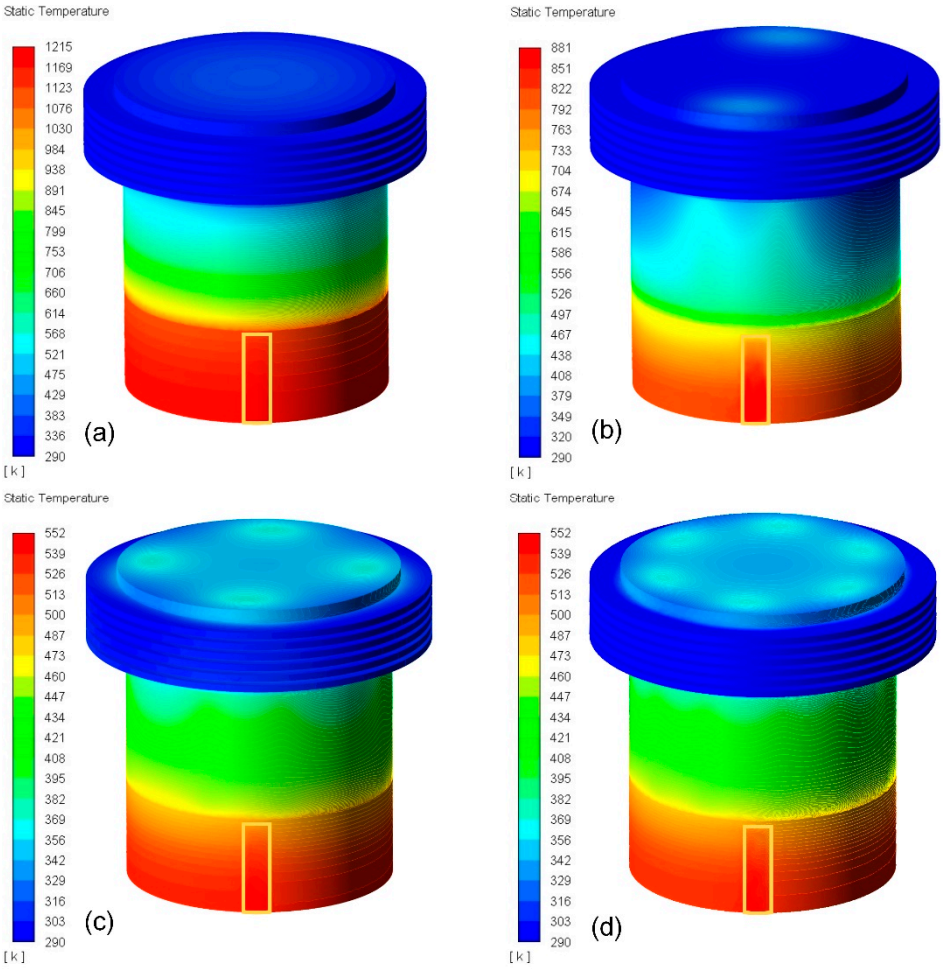

Figure 9. Temperature distribution on the grinding wheel under a grinding heat flux of 10^7 W/m^2: (**a**) 0 OHP, (**b**) 2 OHPs, (**c**) 4 OHPs and (**d**) 6 OHPs (Temperature unit: K).

From the temperature distribution point of view, the grinding zone and abrasive layer have a higher temperature, due to the direct heat load. When away from the abrasive layer, the temperature gets lower. For the grinding wheel without OHP, the heat can only dissipate via the low-conductive matrix and natural convection with the environment. Consequently, the grinding heat gathers in the grinding zone, which leads to a high temperature rise and large temperature difference between the condenser and evaporator. Nevertheless, with the help of OHPs, more and more grinding heat is transferred from the abrasive layer (evaporator) to the condenser, which reduces heat accumulation in the grinding zone. Thereby, both the temperature in the abrasive layer and the temperature difference decrease, which indicates the excellent heat transfer and temperature control abilities. The temperature in the abrasive layer (evaporator) of the grinding wheel without OHPs is the highest, 918 °C, compared with the grinding wheel with 2, 4 and 6 OHPs (587 °C, 346 °C and 277 °C). Then, the temperature drops sharply away from the abrasive layer, while the temperature of the grinding wheel with OHPs decreases gradually. In the condenser, the grinding wheel with 6 OHPs has the highest temperature, followed by the grinding wheel with 4 and 2 OHPs; the grinding wheel without OHPs has the lowest temperature, as shown in Figure 10.

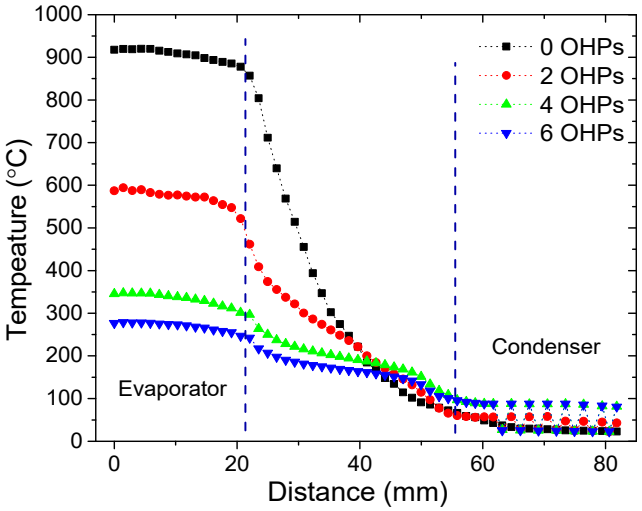

Figure 10. Temperature on the grinding wheel along the axial direction (10^7 W/m^2).

The grinding heat transfer process can be revealed by the temperature field on the grinding wheel, as shown in Figure 11. For the grinding wheel with 6 OHPs under 10^7 W/m^2, at the initial moment, the temperature of the grinding wheel is at the initial temperature, 15 °C. As soon as the grinding process starts, the heat transfers into the abrasive layer, and in 0.5 s the temperature in the abrasive layer reaches 100 °C. In less than 1 s, the heat is transferred to the condenser via the OHPs, and the temperature near the OHPs is higher than for other regions, as shown in Figure 11. Along with the heat transport, the overall temperature of the grinding wheel continues to rise. In 20 s, a stable state is achieved. It is clear that OHPs increase the heat transport capacity of the grinding wheel; the isothermal contour on the outer surface is in a wavy shape, and the temperature near OHPs is higher.

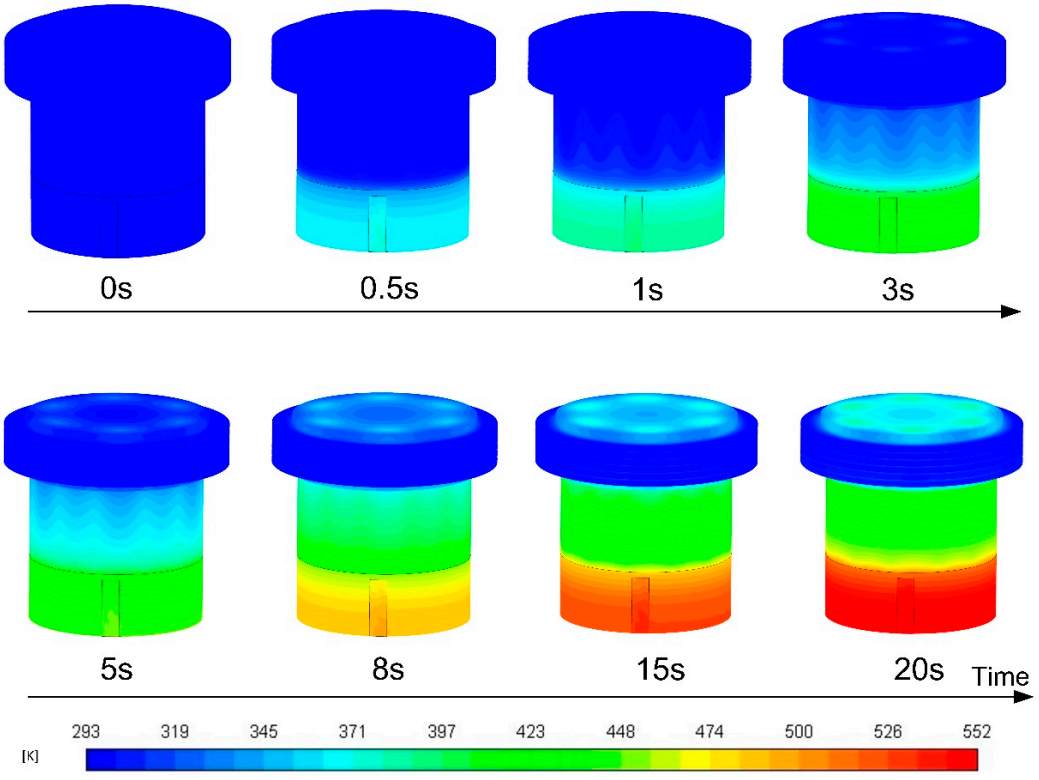

Figure 11. Changes of temperature on the grinding wheel with 6 OHPs (Temperature unit: K).

3.3. Temperature Field of the Workpiece

The inside OHPs increase the heat transport capacity of the grinding wheel, and further change the heat partition of the grinding processes. Less grinding heat will gather in the grinding zone and transfer into the workpiece. The temperature distribution on the workpiece is focused on in this section.

Likewise, on the workpiece, the temperature in the grinding zone is the highest because the thermal conduction of the Ti-6Al-4V workpiece is low, 9.8 W/(m·K). Additionally, there is a large temperature gradient between the grinding zone and outside. Besides, for the grinding wheels with and without OHPs, the temperature distribution on the workpiece is similar, as illustrated in Figure 12.

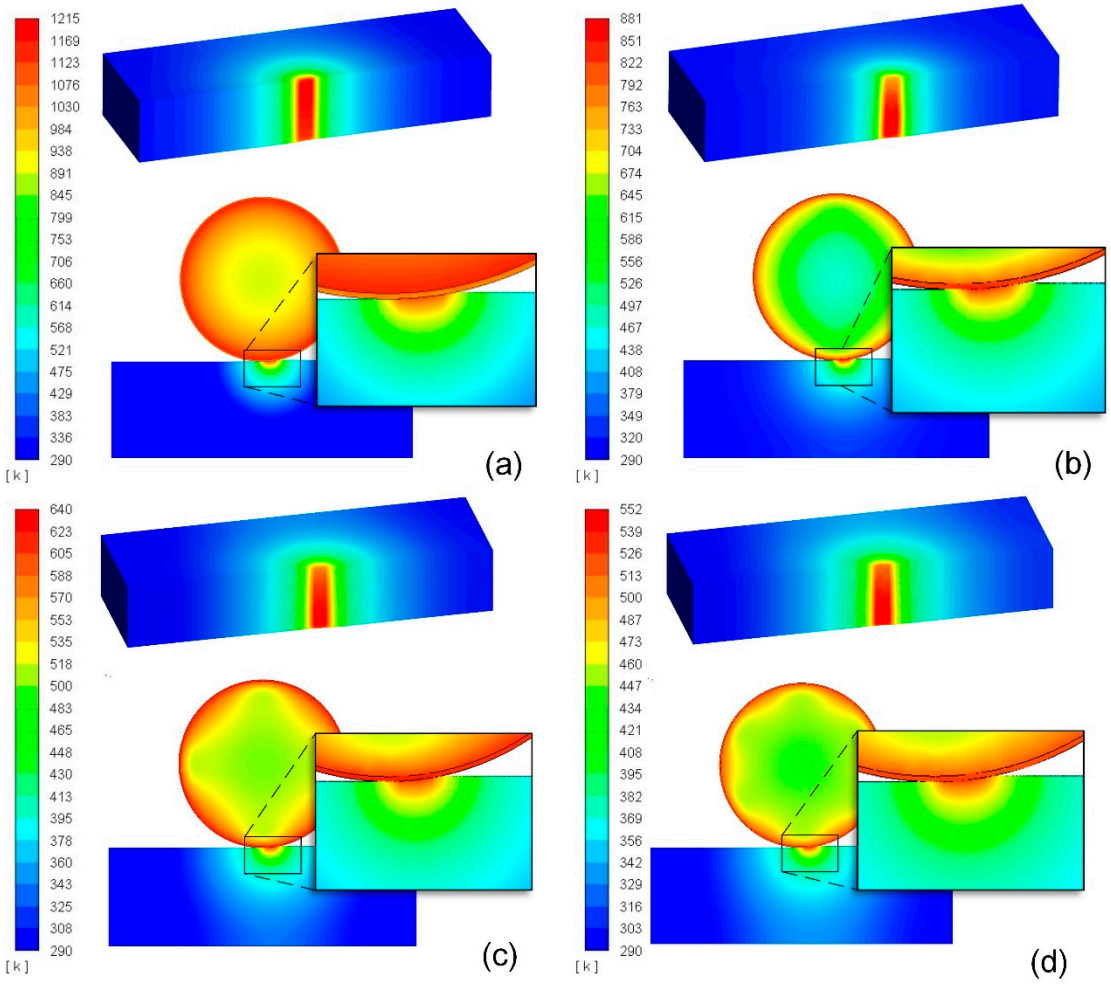

Figure 12. Temperature distribution on the workpiece under a grinding heat flux of 10^7 W/m^2: (**a**) non-OHP, (**b**) 2 OHPs, (**c**) 4 OHPs and (**d**) 6 OHPs (Temperature unit: K).

The temperature along the ground surface direction on the workpiece is captured as shown in Figure 13. Point P in Figure 13 is the point on the boundary of the grinding zone and the ground surface; hence, the temperature at point P is chosen as the temperature of the ground surface, which is not cooled by the natural convection of the environment. The temperature on the selected line can reveal the temperature on the ground surface, which is cooled by the environment, the temperature in the grinding zone and the temperature inside the workpiece.

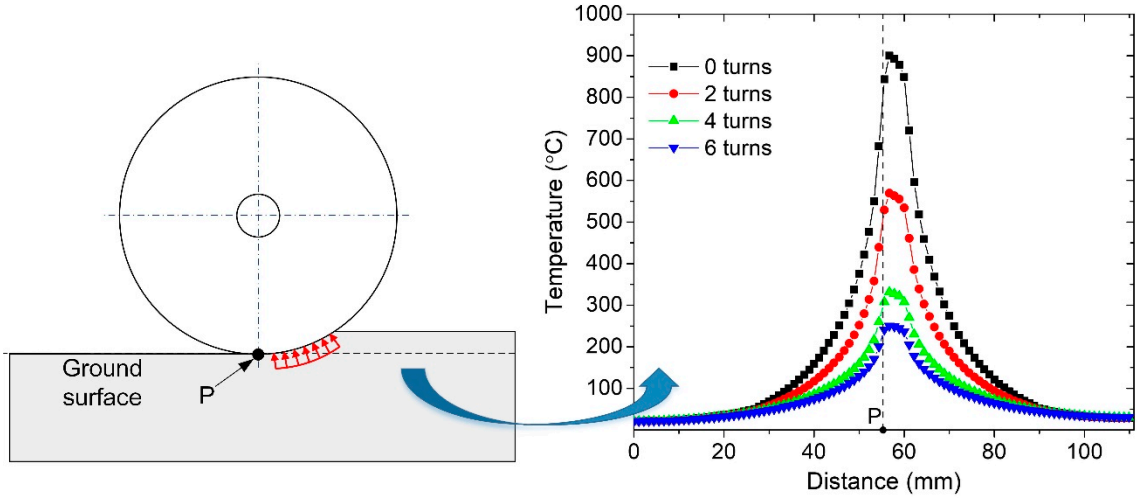

Figure 13. Temperature distribution on the ground surface under a grinding heat flux of 10^7 W/m^2.

Under a grinding heat flux of 10^7 W/m^2, both the temperature in the grinding zone and the temperature on the ground surface decrease with the increase of OHP numbers. When the number of OHPs increases from 0 to 4, the temperature on the workpiece drops dramatically. When the OHP number further increases to 6, the temperature decreases slowly, as demonstrated in Figure 14. The temperature of the ground surface generated by the grinding wheel without OHP is 823.3 °C, while when using the grinding wheels with 2, 4 and 6 OHPs the temperatures are 507 °C, 301 °C and 237 °C, dropping by 38.5%, 63.5% and 71.2%. The enhanced heat transfer effect of the OHP grinding wheel is significant.

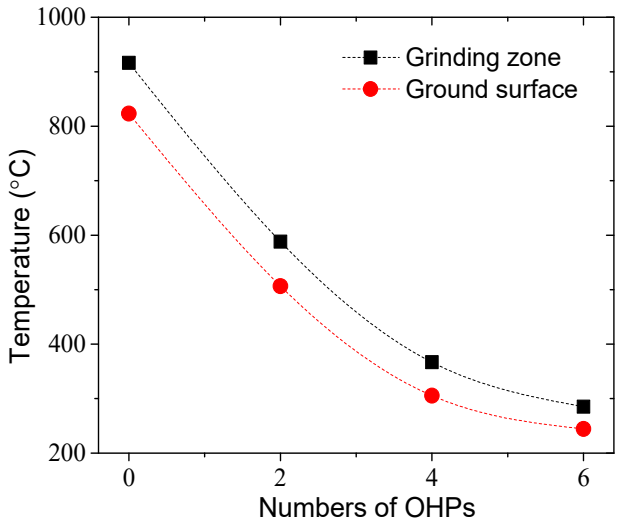

Figure 14. The highest temperature in the grinding zone and the ground surface temperature under a grinding heat flux of 10^7 W/m^2.

4. Conclusions

A numerical analysis is conducted in this paper to figure out the temperature distribution on the grinding wheel and the workpiece during the grinding process by the novel oscillating heat pipe grinding wheel. To investigate the enhanced heat transport capacity and temperature control ability, four oscillating heat pipe grinding wheels are involved, namely the grinding wheel without oscillating heat pipe, and the grinding wheels with 2, 4 and 6 oscillating heat pipes. The three-dimensional

thermal conduction model is built accordingly, containing the grinding wheel, grinding zone and Ti-6Al-4V workpiece.

The temperature fields under grinding heat flux values ranging from 3×10^6 W/m^2 to 1×10^7 W/m^2 are calculated. Along with the increase of the grinding heat flux, the highest temperature in the grinding zone and the temperature difference between the abrasive layer and the condenser of the grinding wheel rise almost linearly. When more oscillating heat pipes are applied, the heat transfer ability of the grinding wheel improves and the grinding temperature decreases. Comparing the grinding wheels with 0 and 6 oscillating heat pipes, the temperature in the grinding zone decreases from 917 °C to 286 °C by 68.7% under 1×10^7 W/m^2. A grinding wheel with a high thermal transfer ability changes the heat partition in the grinding process. Given the development of the grinding temperature, the grinding heat preferentially transfers to the grinding wheel. More grinding heat is carried away by the grinding wheel, and therefore less grinding heat gathers in the grinding zone or transfers into the workpiece. As a result, the temperature on the ground surface decreases significantly; for example, the temperature on the ground surface decreases from 823 °C to 244 °C by 70.4% when shifting from a grinding wheel without oscillating heat pipes to one with 6 oscillating heat pipes under 1×10^7 W/m^2. Furthermore, according to the simulation analysis, in the future, OHP grinding wheels will be fabricated, and experiments using dry-grinding titanium alloy via OHP grinding wheels will be conducted.

Author Contributions: Conceptualization, N.Q. and Z.Z.; methodology, Z.Z.; software, N.Q.; validation, N.Q. and Z.Z.; formal analysis, Z.Z.; investigation, N.Q. and J.C.; writing—original draft preparation, N.Q. and Z.Z.; writing—review and editing, Y.F. and J.X.; supervision, J.X.; funding acquisition, J.X. and J.C. All authors have read and agreed to the published version of the manuscript.

Funding: This research was funded by the National Natural Science Foundation of China (Grant No. 51905275). National Natural Science Foundation of China for Creative Research Group (Grant No. 51921003). Natural Science Foundation of Jiangsu Province (Grant No. BK20190752) and Natural Science Foundation of Colleges and Universities in Jiangsu Province (Grant No. 19KJB460020).

Acknowledgments: Authors would like to thank Guoqing You for his assistance with the software.

Conflicts of Interest: The authors declare no conflict of interest.

Nomenclature

a_p	Depth of cut, mm
b	Width of grinding wheel, mm
d_s	Diameter of the grinding wheel, mm
d_0	Hydraulic diameter of the oscillating heat pipe channel, mm
F_t	Tangential grinding force, N
k_a	Thermal conduction of the abrasive layer, W/(m·K)
k_m	Thermal conduction of the matrix of the grinding wheel, W/(m·K)
k_{OHP}	Thermal conduction of the oscillating heat pipe grinding wheel, W/(m·K)
L_a	Thickness of the matrix of the grinding wheel, mm
L_m	Thickness of the matrix of the grinding wheel, mm
L_{total}	Thickness of the matrix of the evaporation of the grinding wheel, mm
l_s	Length of the grinding zone, mm
N	Length of the grinding zone, mm
P	Power, W
Q_{total}	Total grinding heat flux, W/m^2
v_s	Grinding speed, m/s
v_w	Infeed speed, mm/min

References

1. Prasad Rambabu, N.; Eswara Prasad, V.V.K.; Wanhill, R.J.H. *Aerospace Materials and Material Technologies*; Springer: Singapore, 2017; Volume 1, ISBN 9789811021343.
2. Zhang, X.; Chen, Y.; Hu, J. Recent advances in the development of aerospace materials. *Prog. Aerosp. Sci.* **2018**, *97*, 22–34. [CrossRef]
3. Österle, W.; Li, P.X. Mechanical and thermal response of a nickel-base superalloy upon grinding with high removal rates. *Mater. Sci. Eng. A* **1997**, *238*, 357–366. [CrossRef]
4. Malkin, S.; Guo, C. Thermal Analysis of Grinding. *CIRP Ann.* **2007**, *56*, 760–782. [CrossRef]
5. Kappmeyer, G.; Hubig, C.; Hardy, M.; Witty, M.; Busch, M. Modern Machining of Advanced Aerospace Alloys-Enabler for Quality and Performance. *Procedia CIRP* **2012**, *1*, 28–43. [CrossRef]
6. Klocke, F.; Soo, S.L.; Karpuschewski, B.; Webster, J.A.; Novovic, D.; Elfizy, A.; Axinte, D.A.; Tönissen, S. Abrasive machining of advanced aerospace alloys and composites. *CIRP Ann.* **2015**, *64*, 581–604. [CrossRef]
7. Adrian, P. Mouritz Processing and machining of aerospace metals. In *Introduction to Aerospace Materials*; Mouritz, A.P., Ed.; Woodhead Publishing: Cambridge, UK, 2012; pp. 154–172. ISBN 9781855739468.
8. Tawakoli, T.; Rabiey, M. An innovative concept and its effects on wheel surface topography in dry grinding by resin and vitrified bond CBN wheel. *Mach. Sci. Technol.* **2008**, *12*, 514–528. [CrossRef]
9. Malkin, S. Current Trends in CBN Grinding Technology. *CIRP Ann. Manuf. Technol.* **1985**, *34*, 557–563. [CrossRef]
10. Chen, S.P.; Liu, X.P.; Wan, L.; Gao, P.Z.; Zhang, W.; Hou, Z.Q. Effect of V_2O_5 addition on the wettability of vitrified bond to diamond abrasive and grinding performance of diamond wheels. *Diam. Relat. Mater.* **2020**, *102*, 107672. [CrossRef]
11. Zhi, G.; Bi, W.Y.; Tang, J.J.; Rong, Y.K. The analysis of bonding mechanism of CBN grains for electroplated superabrasive tools. In Proceedings of the Applied Mechanics and Materials, Jakarta, Indonesia, 15–16 October 2014.
12. Li, Z.; Ding, W.; Shen, L.; Xi, X.; Fu, Y. Comparative investigation on high-speed grinding of TiCp/Ti–6Al–4V particulate reinforced titanium matrix composites with single-layer electroplated and brazed CBN wheels. *Chin. J. Aeronaut.* **2016**, *29*, 1414–1424. [CrossRef]
13. Lyu, J.J.; Wu, X.; Liu, Y.; Liu, Y.; Li, A.D.R.; Zheng, Y.; Shih, A. A miniature nickel-diamond electroplated wheel for grinding of the arterial calcified plaque. In Proceedings of the Procedia Manufacturing, Penn State Behrend Erie, PA, USA, 10–14 June 2019.
14. Marinescu, I.D.; Rowe, W.B.; Dimitrov, B.; Ohmori, H. *Tribology of Abrasive Machining Processes*; Elsevier: Oxford, UK, 2012; ISBN 9781437734676.
15. Ren, B.; Gao, L.; Xie, B.T.; Li, M.J.; Zhang, S.D.; Zu, G.Q.; Ran, X. Tribological properties and anti-wear mechanism of ZnO@graphene core-shell nanoparticles as lubricant additives. *Tribol. Int.* **2020**, *144*, 106114. [CrossRef]
16. Zhang, Z.; Yao, P.; Li, X.; Wang, J.; Huang, C.; Zhu, H.; Zou, B.; Liu, H. Grinding performance and tribological behavior in solid lubricant assisted grinding of glass-ceramics. *J. Manuf. Process.* **2020**, *51*, 31–43. [CrossRef]
17. Kuang, W.; Zhao, B.; Yang, C.; Ding, W. Effects of h-BN particles on the microstructure and tribological property of self-lubrication CBN abrasive composites. *Ceram. Int.* **2020**, *46*, 2457–2464. [CrossRef]
18. Hadad, M.J.; Tawakoli, T.; Sadeghi, M.H.; Sadeghi, B. Temperature and energy partition in minimum quantity lubrication-MQL grinding process. *Int. J. Mach. Tools Manuf.* **2012**, *54–55*, 10–17. [CrossRef]
19. Sadeghi, M.H.; Haddad, M.J.; Tawakoli, T.; Emami, M. Minimal quantity lubrication-MQL in grinding of Ti–6Al–4V titanium alloy. *Int. J. Adv. Manuf. Technol.* **2009**, *44*, 487–500. [CrossRef]
20. Damir, A.; Shi, B.; Attia, M.H. Flow characteristics of optimized hybrid cryogenic-minimum quantity lubrication cooling in machining of aerospace materials. *CIRP Ann.* **2019**, *68*, 77–80. [CrossRef]
21. Li, B.; Li, C.; Zhang, Y.; Wang, Y.; Jia, D.; Yang, M. Grinding temperature and energy ratio coefficient in MQL grinding of high-temperature nickel-base alloy by using different vegetable oils as base oil. *Chin. J. Aeronaut.* **2016**, *29*, 1084–1095. [CrossRef]
22. Shen, B.; Kalita, P.; Malshe, A.P.; Shih, A.J. Performance of novel MoS_2 nanoparticles based grinding fluids in minimum quantity lubrication grinding. In Proceedings of the Transactions of the North American Manufacturing Research Institution of SME, Monterry, Mexico, 20–23 May 2008; Volume 36, pp. 357–364.

23. Jia, D.; Li, C.; Wang, S.; Zhang, Q.; Hou, Y. Advances and Patents about Grinding Equipments with Nano-Particle Jet Minimum Quantity Lubrication. *Recent Pat. Nanotechnol.* **2015**, *8*, 215–229. [CrossRef]
24. Singh, H.; Sharma, V.S.; Singh, S.; Dogra, M. Nanofluids assisted environmental friendly lubricating strategies for the surface grinding of titanium alloy: Ti6Al4V-ELI. *J. Manuf. Process.* **2019**, *39*, 241–249. [CrossRef]
25. Setti, D.; Ghosh, S.; Paruchuri, V.R. Influence of nanofluid application on wheel wear, coefficient of friction and redeposition phenomenon in surface grinding of Ti-6Al-4V. *Proc. Inst. Mech. Eng. Part. B J. Eng. Manuf.* **2018**, *232*, 128–140. [CrossRef]
26. Singh, H.; Sharma, V.S.; Dogra, M. Exploration of graphene assisted vegetables oil based minimum quantity lubrication for surface grinding of TI-6AL-4V-ELI. *Tribol. Int.* **2020**, *144*, 106113. [CrossRef]
27. Li, M.; Yu, T.; Zhang, R.; Yang, L.; Ma, Z.; Li, B.; Wang, X.Z.; Wang, W.; Zhao, J. Experimental evaluation of an eco-friendly grinding process combining minimum quantity lubrication and graphene-enhanced plant-oil-based cutting fluid. *J. Clean. Prod.* **2020**, *244*, 118747. [CrossRef]
28. Shibata, J.; Yonetsu, S. Thermal Aspects of Creep-Feed Grinding and Effective Coolant Application. In Proceedings of the Twenty-Sixth International Machine Tool Design and Research Conference, Manchester, UK, 17–18 September 1986.
29. Chong-Ching, C. An application of lubrication theory to predict useful flow-rate of coolants on grinding porous media. *Tribol. Int.* **1997**, *30*, 575–581. [CrossRef]
30. Cayli, T.; Klocke, F.; Döbbeler, B. Increasing Energy Efficiency in Turning of Aerospace Materials with High-Pressure Coolant Supply. *Procedia Manuf.* **2018**, *21*, 405–412. [CrossRef]
31. Zhang, J.; Li, C.; Zhang, Y.; Yang, M.; Jia, D.; Liu, G.; Hou, Y.; Li, R.; Zhang, N.; Wu, Q.; et al. Experimental assessment of an environmentally friendly grinding process using nanofluid minimum quantity lubrication with cryogenic air. *J. Clean. Prod.* **2018**, *193*, 236–248. [CrossRef]
32. Setti, D.; Yadav, N.K.; Ghosh, S. Grindability improvement of Ti-6Al-4V using cryogenic cooling. *Proc. Inst. Mech. Eng. Part. B J. Eng. Manuf.* **2014**, *228*, 1131–1137. [CrossRef]
33. Amini, S.; Baraheni, M.; Esmaeili, S.J. Experimental comparison of MO40 steel surface grinding performance under different cooling techniques. *Int. J. Light. Mater. Manuf.* **2019**, *2*, 330–337. [CrossRef]
34. Du, Z.; Zhang, F.; Xu, Q.; Huang, Y.; Li, M.; Huang, H.; Wang, C.; Zhou, Y.; Tang, H. Selective laser sintering and grinding performance of resin bond diamond grinding wheels with arrayed internal cooling holes. *Ceram. Int.* **2019**, *45*, 20873–20881. [CrossRef]
35. Li, X.; Chen, Z.; Chen, W. Suppression of surface burn in grinding of titanium alloy TC4 using a self-inhaling internal cooling wheel. *Chin. J. Aeronaut.* **2011**, *24*, 96–101. [CrossRef]
36. Kirsch, B. The impact of contact zone flow rate and bulk cooling on the cooling efficiency in grinding applying different nozzle designs and grinding wheel textures. *CIRP J. Manuf. Sci. Technol.* **2017**, *18*, 179–187. [CrossRef]
37. Yang, M.; Li, C.; Zhang, Y.; Wang, Y.; Li, B.; Jia, D.; Hou, Y.; Li, R. Research on microscale skull grinding temperature field under different cooling conditions. *Appl. Therm. Eng.* **2017**, *126*, 525–537. [CrossRef]
38. Webster, J.; Brinksmeier, E.; Heinzel, C.; Wittmann, M.; Thoens, K. Assessment of Grinding Fluid Effectiveness in Continuous-Dress Creep Feed Grinding. *CIRP Ann.* **2002**, *51*, 235–240. [CrossRef]
39. Kim, J.; Hwang, J.; Jung, Y. Development of twin wheel creep-feed grinding machine using continuous dressing for machining of aircraft rotary wing. *J. Cent. South. Univ.* **2011**, *18*, 704–710. [CrossRef]
40. Zhao, Z.; Xu, J.; Fu, Y. Study on coolant-induced hydrodynamic pressure in contact zone while deep grinding with CBN wheels. *Mach. Sci. Technol.* **2016**, *20*, 547–566. [CrossRef]
41. Ma, H. *Oscillating Heat Pipes*; Springer: New York, NY, USA, 2015; ISBN 9781493925049.
42. Jo, J.; Kim, J.; Kim, S.J. Experimental investigations of heat transfer mechanisms of a pulsating heat pipe. *Energy Convers. Manag.* **2019**, *181*, 331–341. [CrossRef]
43. Qian, N.; Fu, Y.; Zhang, Y.; Chen, J.; Xu, J. Experimental investigation of thermal performance of the oscillating heat pipe for the grinding wheel. *Int. J. Heat Mass Transf.* **2019**, *136*, 911–923. [CrossRef]
44. Taft, B.S.; Williams, A.D.; Drolen, B.L. Review of Pulsating Heat Pipe Working Fluid Selection. *J. Thermophys. Heat Transf.* **2012**, *26*, 651–656. [CrossRef]
45. Creatini, F.; Guidi, G.M.; Belfi, F.; Cicero, G.; Fioriti, D.; Di Prizio, D.; Piacquadio, S.; Becatti, G.; Orlandini, G.; Frigerio, A.; et al. Pulsating Heat pipe only for Space (PHOS): Results of the REXUS 18 sounding rocket campaign. *J. Phys. Conf. Ser.* **2015**, *655*. [CrossRef]

46. Qu, J.; Sun, Q.; Wang, H.; Zhang, D.; Yuan, J. Performance characteristics of flat-plate oscillating heat pipe with porous metal-foam wicks. *Int. J. Heat Mass Transf.* **2019**, *137*, 20–30. [CrossRef]
47. Wu, Z.; Deng, J.; Su, C.; Luo, C.; Xia, D. Performance of the micro-texture self-lubricating and pulsating heat pipe self-cooling tools in dry cutting process. *Int. J. Refract. Met. Hard Mater.* **2014**, *45*, 238–248. [CrossRef]
48. Wu, Z.; Yang, Y.; Luo, C. Design, fabrication and dry cutting performance of pulsating heat pipe self-cooling tools. *J. Clean. Prod.* **2016**, *124*, 276–282. [CrossRef]
49. Qian, N.; Fu, Y.; Marengo, M.; Chen, J.; Xu, J. Start-up timing behavior of single-loop oscillating heat pipes based on the second-order dynamic model. *Int. J. Heat Mass Transf.* **2020**, *147*, 118994. [CrossRef]
50. Qian, N.; Wang, X.; Fu, Y.; Zhao, Z.; Xu, J.; Chen, J. Predicting heat transfer of oscillating heat pipes for machining processes based on extreme gradient boosting algorithm. *Appl. Therm. Eng.* **2020**, *164*, 114521. [CrossRef]
51. Ebrahimi Dehshali, M.; Nazari, M.A.; Shafii, M.B. Thermal performance of rotating closed-loop pulsating heat pipes: Experimental investigation and semi-empirical correlation. *Int. J. Therm. Sci.* **2018**, *123*, 14–26. [CrossRef]
52. Aboutalebi, M.; Nikravan Moghaddam, A.M.; Mohammadi, N.; Shafii, M.B. Experimental investigation on performance of a rotating closed loop pulsating heat pipe. *Int. Commun. Heat Mass Transf.* **2013**, *45*, 137–145. [CrossRef]
53. Liou, T.-M.; Chang, S.W.; Cai, W.L.; Lan, I.-A. Thermal fluid characteristics of pulsating heat pipe in radially rotating thin pad. *Int. J. Heat Mass Transf.* **2019**, *131*, 273–290. [CrossRef]
54. On-ai, K.; Kammuang-lue, N.; Terdtoon, P.; Sakulchangsatjatai, P. Implied physical phenomena of rotating closed-loop pulsating heat pipe from working fluid temperature. *Appl. Therm. Eng.* **2019**, *148*, 1303–1309. [CrossRef]
55. Qian, N.; Fu, Y.; Marengo, M.; Xu, J.; Chen, J.; Jiang, F. Heat Transport Capacity of an Axial-Rotating Single-Loop Oscillating Heat Pipe for Abrasive-Milling Tools. *Energies* **2020**, *13*, 2145. [CrossRef]
56. Klocke, F. *Manufacturing Processes 2. Grinding, Honing, Lapping*; Springer: Berlin/Heidelberg, Germany, 2013; ISBN 9788578110796.